Article

Dynamic Motions of the HIV-1 Frameshift Site RNA

Kathryn D. Mouzakis,[1] Elizabeth A. Dethoff,[2] Marco Tonelli,[1] Hashim Al-Hashimi,[3] and Samuel E. Butcher[1,*]
[1]Department of Biochemistry, University of Wisconsin-Madison, Madison, Wisconsin; [2]Department of Chemistry, University of North Carolina, Chapel Hill, North Carolina; and [3]Department of Chemistry, Duke University, Durham, North Carolina

ABSTRACT The HIV-1 frameshift site (FS) plays a critical role in viral replication. During translation, the HIV-1 FS transitions from a 3-helix to a 2-helix junction RNA secondary structure. The 2-helix junction structure contains a GGA bulge, and purine-rich bulges are common motifs in RNA secondary structure. Here, we investigate the dynamics of the HIV-1 FS 2-helix junction RNA. Interhelical motions were studied under different ionic conditions using NMR order tensor analysis of residual dipolar couplings. In 150 mM potassium, the RNA adopts a 43°(±4°) interhelical bend angle (β) and displays large amplitude, anisotropic interhelical motions characterized by a 0.52(±0.04) internal generalized degree of order (GDO_{int}) and distinct order tensor asymmetries for its two helices (η = 0.26(±0.04) and 0.5(±0.1)). These motions are effectively quenched by addition of 2 mM magnesium (GDO_{int} = 0.87(±0.06)), which promotes a near-coaxial conformation (β = 15°(±6°)) of the two helices. Base stacking in the bulge was investigated using the fluorescent purine analog 2-aminopurine. These results indicate that magnesium stabilizes extrahelical conformations of the bulge nucleotides, thereby promoting coaxial stacking of helices. These results are highly similar to previous studies of the HIV transactivation response RNA, despite a complete lack of sequence similarity between the two RNAs. Thus, the conformational space of these RNAs is largely determined by the topology of their interhelical junctions.

INTRODUCTION

RNA structures are composed of A-form helical domains connected by bulges, single-stranded linkers, internal loops, and nonhelical motifs (1). The connections between helices allow RNA structures to adopt an ensemble of conformations that are sampled through interhelical motions on the nanosecond to millisecond timescale (2–6). Changes in the relative orientation of helical domains are often observed during functionally important RNA conformational transitions including folding, adaptive recognition, and catalysis (7–11). RNA bulges are an extremely common structural motif and occur when two covalently connected helices are interrupted by a single stretch of unpaired nucleotides (12–15).

The boundaries of allowed RNA interhelical conformational space are determined by simple topological constraints such as covalent connectivity, stereochemistry, and steric clash. Furthermore, the observed distribution of interhelical conformations in the Protein Data Bank (PDB) mirrors the topologically allowed space (6). However, sequence-specific conformational preferences and dynamic motions are also known to exist (16–18). Little is known about how sequence impacts the highly correlated bending and twisting motions associated with RNA bulges (19). Flanking basepairs may also have a large effect on RNA dynamics (4,6,20).

Despite the enormous size and diversity of RNA transcriptomes (21–23), most of what is known about RNA dynamics has been derived from a relatively small collection of RNAs (19,24–35). Among these, the HIV-1 transactivation response (TAR) RNA element has been studied extensively and has served as a model for investigating RNA motional amplitudes and dynamics (2,4,6,19,20,36–46). TAR contains two helices separated by a flexible three-pyrimidine (UCU) bulge. In low-ionic strength conditions, TAR has an interhelical bend angle of 47°(±5°) (18,37), is flexible (36), and samples a wide but anisotropic range of conformations (6,20,46) that feature spatially correlated twisting and bending motions (46). Interestingly, the addition of magnesium has a striking effect on the interhelical motions of TAR, resulting in coaxial stacking and quenching of interhelical motions (37). These results can be described with a simple two-state model (40) where stacking of the bulge nucleotides separates the phosphate charges in the UCU bulge, resulting in a bent but flexible interhelical conformation favored by low to moderate concentrations of monovalent ions. Magnesium ions effectively shield the negatively charged phosphate groups in the bulge, allowing them to move closer together to facilitate unstacking of nucleotides and resulting in a more rigid coaxial state (40). Recent molecular dynamics (MD) simulations of the TAR UCU bulge suggest that interhelical dynamics involve at least three clusters of bulge ensembles that display different hydrogen bonding patterns and degrees of stacking (16).

Submitted July 7, 2014, and accepted for publication December 5, 2014.

*Correspondence: sebutcher@wisc.edu

Kathryn D. Mouzakis's present address is Department of Chemistry, Fort Lewis College, Durango, CO 81301.

Editor: Michael Sattler.

0006-3495/15/02/0644/11 $2.00

http://dx.doi.org/10.1016/j.bpj.2014.12.006

It is not yet clear whether the large amplitude dynamic motions of TAR (19,36) and their modulation by counterions (3,37–40) are sequence-specific or reflect a more general feature of trinucleotide bulges. Changing the sequence identity of a Watson-Crick basepair flanking the TAR bulge from A-U to a more stable G-C significantly diminishes the amplitude of interhelical motions (17), supporting the idea of sequence-dependent bulge dynamics. Indeed, MD simulations suggest that adjacent basepair opening rates may affect bulge dynamics (16). Transient electric birefringence studies of RNA helices connected by A and U bulges of varying lengths revealed that magnesium ions differentially affect the bend angle of poly-U versus poly-A bugles (18). In contrast, magnesium was observed to have no impact on the average interhelical bend angle or dynamics of the RNase P P4 domain, which has a single uridine bulge (47).

The thermodynamic stability of bulges is likely to play an important role in RNA interhelical motions. Although the free energies for RNA dinucleotide steps within duplex RNAs depend upon nearest-neighbor interactions (48–50), the thermodynamic stability of bulges can be influenced by distal (non-nearest-neighbor) tertiary interactions (51–54). The thermodynamic contribution of single nucleotide stacking is always small for nucleotides 5′ of a helical end, and depends on sequence for nucleotides 3′ of a helical end (55–57). This is due to the right-handed nature of the RNA helix, which exhibits more stacking for 3′ vs. 5′ terminal nucleotides (58). In general, 3′ purines are more stabilizing than pyrimidines (56,57). Therefore, purine bulges are expected to have higher stacking propensities than pyrimidine bulges, and these differences may significantly influence interhelical dynamics. A MD study estimated that unstacking of a single bulged adenosine from within an RNA helix costs an additional ~1.5 kcal/mol of free energy relative to flipping a uridine nucleotide into solution (59). The sequence-dependent thermodynamics of di- and trinucleotide bulges, and their impact on interhelical domain motions, have yet to be systematically investigated.

Dynamic motions occurring over the course of picoseconds to milliseconds can be studied by NMR measurements of residual dipolar couplings (RDCs) (3,5,60–64). These couplings report angular information on the weighted average of all conformations sampled by a macromolecule. The long-range information derived from RDCs can be used to efficiently quantify helical orientation and dynamics in a variety of solution conditions (5). However, the coupling of internal and overall domain motions can complicate the interpretation of RDCs (2,65,66). This situation becomes most problematic when internal motions alter the overall molecular alignment such that the ordering of both domains is indistinguishable, which interferes with the quantification of interhelical motions (43,67). RDC measurements on artificially elongated helices have proven exceptional at decoupling overall motions from internal motions because the overall alignment of an extended domain is less sensitive to internal motions (2,19,43,45). However, unnaturally long helical extensions are not necessary, as even moderate differences in helical lengths can be sufficient to uncouple these motions (16,43).

Here, we investigate the dynamics of the HIV-1 frameshift site (FS) RNA (63,68–72). During translation of the FS, the RNA switches from a 3-helix junction structure to a 2-helix junction via ribosome-mediated remodeling of the RNA secondary structure (63). The 2-helix junction form of this RNA has been shown to fold into an extremely stable upper helix separated from a lower helix by a GGA bulge (69,72,73) (Fig. 1 *A*). NMR and fluorescence spectroscopy were employed to examine conformational dynamics as a function of potassium and magnesium cation concentrations. We find that, in potassium buffer alone, the RNA adopts an average interhelical bend angle (β) of ~44° and experiences large amplitude domain motions. These dynamics are largely quenched upon addition of 2 mM magnesium. Addition of 2 mM magnesium to RNA in 20 mM potassium promotes a decrease in the interhelical bend angle to ~27° and leads to a higher degree of unstacking of the central purine, as determined by fluorescence of 2-amino purine substituted RNA. These results are surprisingly similar to previous studies of TAR (37,40), although the TAR bulge is UCU, the FS bulge is GGA, and the closing basepairs are different.

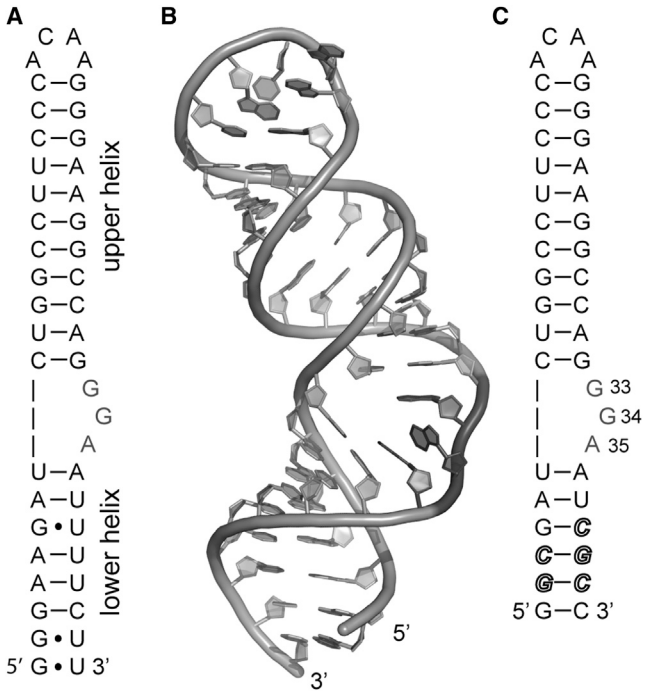

FIGURE 1 RNA constructs used to investigate the HIV-1 FS dynamics. (*A*) The HIV-1 FS consensus sequence, (*B*) solution structure (PDB ID 1Z2J), and (*C*) secondary structure of the modified FS.

MATERIALS AND METHODS

RNA synthesis and purification

The consensus sequence for the lower helix of the HIV-1 FS (Fig. 1 *A*) was modified and truncated (see Fig. 1 *C*) for optimal alignment of the longer, upper helix in Pf1 phage. The synthetic oligonucleotide (5′-TTCTAATAC GACTCACTATAGGCGATCTGGCCTTCCCACAAGGGAAGGCCAGG GAATCGCC-3′) and its complement were purchased (Integrated DNA Technologies (IDT)) and used as a template for in vitro transcription.

RNA for NMR was transcribed in vitro using purified His_6-tagged T7 RNA polymerase and synthetic DNA oligonucleotides (IDT), as previously described (69,71,74). $^{13}C/^{15}N$-labeled RNA was prepared using $^{13}C/^{15}N$-labeled rNTPs (Cambridge Isotope Laboratories). RNA was purified using 12.5% denaturing polyacrylamide gel electrophoresis, identified by ultraviolet absorbance, and excised from the gel. RNA was recovered by diffusion into 0.3 M sodium acetate, precipitated with ethanol, purified on a High-Q anion exchange column (Bio-Rad), again precipitated with ethanol, and desalted on a sephadex G-15 (Sigma) gel filtration column. The purified RNA was lyophilized, resuspended in 20 mM KH_2PO_4 (pH 6.8), and exchanged into each NMR buffer by dialysis against 2 L of buffer at 4°C. Partial alignment of RNA for RDC measurements was achieved by adding Pf1 filamentous bacteriophage (ASLA, Riga, Latvia) at a final concentration of ~10–15 mg/mL to $^{13}C/^{15}N$-labeled samples. RNA used in fluorescence experiments was purchased from IDT.

NMR spectroscopy

All NMR spectra were obtained on a Varian 900 MHz or Bruker 700 MHz spectrometer at the National Magnetic Resonance Facility at Madison (NMRFAM). The spectrometers were equipped with *z*-axis pulsed field gradient cryogenically cooled probes. Chemical shifts were referenced to 2,2-dimethyl-2-silapentane-5-sulfonate (DSS) by adding 2 μM sodium DSS directly to the samples. RDCs were measured in four different solution conditions: 20 mM potassium phosphate (the 20 mM potassium condition) alone or supplemented with either 130 mM potassium chloride (the 150 mM potassium condition), 2 mM magnesium chloride (the 20 mM potassium and 2 mM magnesium condition), or 130 mM potassium chloride and 2 mM magnesium chloride (the 150 mM potassium and 2 mM magnesium condition), all at pH 6.8. ^{1}H-^{13}C-S^3A-heteronuclear single quantum coherence (HSQC), ^{1}H-^{13}C-transverse relaxation-optimized spectroscopy (TROSY)-HSQC, and ^{1}H-^{15}N-TROSY-HSQC experiments were used to collect scalar coupling values in isotropic and partially aligned (~10–15 mg/ml buffer-exchanged Pf1 filamentous bacteriophage (ASLA)) samples. RDCs were calculated by determining the difference in scalar coupling values between isotropic and partially aligned samples. RDC errors were calculated using the root mean-square deviation (rmsd) for each bond type in both the direct and indirect dimensions and between duplicate experiments, as described (67). Spin-pair resonance intensities (peak heights) from ^{1}H-^{13}C-HSQC experiments were normalized to the intensity of the corresponding A25, U8, C16, and G27 (or G24 in the 150 mM potassium and 2 mM magnesium condition) spin-pair resonances. Such spin pairs were chosen because they are expected to experience limited motions (5), given their location in an extremely stable upper helix (69), and their completeness in measurement across all conditions.

Order tensor analysis

RDCs measured in the Watson-Crick basepairs in the upper and lower helices were subjected to order tensor analysis using idealized A-form helices as previously described (67) and validated (36,38,75–78). Upper and lower helices were constructed using Insight II (Accelerys). A-form RNA parameters were checked using 3DNA (79). Propeller twist was corrected using an in-house program as described (67). RDCs were fit to the corrected A-form helices and order tensors were determined using RAMAH (77). CH and NH dipolar couplings are normalized in RAMAH to account for the different gyromagnetic ratios of ^{13}C and ^{15}N and the differences in CH and NH bond lengths. RDCs corresponding to basepairs at the top and bottom of each helix were excluded in the fits because of their departure from ideal A-form RNA characteristics (67). To account for differences in alignment between 100% D_2O and 90% H_2O/10% D_2O NMR experiments, the ^{1}H-^{15}N data collected in 90% H_2O/10% D_2O were uniformly scaled such that an identical order tensor solution with and without ^{1}H-^{15}N data was achieved using RAMAH (77), as previously described (19). Order tensor errors due to A-form structural noise and RDC error were calculated using Aform-RDC (78), with the error input being the average RDC error (2–3 Hz, Tables S1–S4 in the Supporting Material). Excellent fits to order tensors were achieved for RDCs measured under all conditions. In all instances, the rmsd compared favorably with the RDC measurement uncertainty.

Order tensor solutions were used to rotate each A-form helix into its principal axis system (PAS) using the program EULER-RNA (67). Order tensor solutions have a 4^{n-1} degeneracy, where n is the number of helices, such that once the helix is in its PAS, rotation by 180° about each principal axis yields three additional degenerate order tensor solutions. To determine the correct helix orientation, two connectivity restraints were used. The first required connectivity between C7-P and U6-O3′ atoms and eliminated two of the four solutions. To satisfy this restraint, the lower helix was translated without rotation such that the average A-form distance separated the C7-P and U6-O3′ atoms (80). Specifically, the U6-O3′ atom was 1.58 Å from the C7-P atom, with a 102° O5′-P-O3′ bond angle and a 62° dihedral angle about the O5′-P bond. A final solution was selected by elimination of the model that violated the distance restraint between the G32-O3′ and A36-P atoms. This distance must be smaller than or equal to the theoretically allowed length of 21 Å (67). Interhelical bend angles (β) and dynamic parameters were calculated in each condition as previously described (67). To specifically compare the motion of one helix relative to the other, the generalized degree of order (GDO) for the dynamic helix was normalized by the GDO for the helix dominating the alignment, giving the internal GDO (GDO_{int}). Motional asymmetry was qualitatively evaluated using η. Twist angles calculated by Euler-RNA have large uncertainties ($\sim\pm50°$) (67), and when the bend angle is near zero, the twist angle cannot be accurately determined. For the 150 mM potassium and 2 mM magnesium condition (15° interhelical bend angle), Euler-RNA predicted a 36° twist, which required an additional −50° rotation about the z axis to avoid steric clash between G32 and A36, producing a final twist of −14°. The principal direction of order (S_{zz}) orientation was determined relative to a molecular frame in which the helical axis of the upper helix is aligned along the z axis.

Fluorescence-monitored nucleotide stacking

Fluorescence measurements were performed in triplicate similar to those previously described (71). Briefly, the 2-aminopurine substituted RNAs (HIV-1 G33-2AP, G34-2AP, and A35-2AP) were excited at 309 nm and emission was measured at 360 nm with a Varian Cary Eclipse Fluorescence spectrometer. Magnesium chloride and potassium chloride were added to 2 mM or 130 mM, respectively, into a 2 μM RNA and 20 mM potassium phosphate buffer (pH 6.8) solution. To measure the impact of magnesium on 2AP fluorescence in a 150 mM potassium background, magnesium chloride was added to 2 mM into a 2 μM RNA, 150 mM potassium solution (20 mM potassium phosphate, 130 mM potassium chloride, pH 6.8). Using a 160 μL sample cell, fluorescence was measured for 2 s, five consecutive times, at 30°C. The average of at least three replicates and standard deviation are reported.

RESULTS AND DISCUSSION

The HIV-1 FS NMR structure is shown (Fig. 1, *A* and *B*) (69). The lower helix was truncated to yield an overall

alignment tensor dominated by the 11 basepair upper helix (Fig. 1 *C*). Resonances were assigned by reference to previous assignments (69), analysis of two-dimensional nuclear Overhauser effect spectroscopy spectra (data not shown), and comparison of HSQC spectra measured in different ionic conditions (Figs. S1 and S2). RDCs measured in different ionic conditions were subjected to order tensor analysis assuming an idealized A-form helix geometry (3,62,67,81). We observed good agreement between the measured and back-predicted RDCs in all four conditions (Table 1: $R^2 = 0.96–0.99$, rmsd = 1.7–3.5 Hz), validating the use of order tensor solutions to describe interhelical dynamics.

In the absence of magnesium, the upper helix was indeed found to dominate the overall alignment as assessed by its much larger GDO (Table 1: GDO = 1.7–2.0) as compared to the shorter helix (Table 1: GDO =1.0–1.1). As expected, the principal axis of the order tensor (S_{zz}) is oriented on average nearly parallel to the axis of the upper helix, with deviations of $7°(\pm 2°)$, $11°(\pm 3°)$, $3°(\pm 1°)$, and $2°(\pm 2°)$ in 20 mM potassium, 150 mM potassium, 20 mM potassium and 2 mM magnesium, and 150 mM potassium and 2 mM magnesium, respectively.

In potassium alone, the RDCs measured for the lower helix are on average, decreased in magnitude relative to the upper helix (Fig. 2, *A–C*). These data are consistent with large amplitude domain motions of the lower helix relative to the upper helix, which dominates the alignment under variable potassium concentrations. In both magnesium conditions, the degree of alignment of the upper and lower helices (Table 1, GDO), as well as the magnitude of the RDCs (Fig. 2, *D* and *E*), is similar. This can be attributed to either quenching of the interhelical motions upon addition of magnesium or a motionally coupled state (43), the latter being much less likely given the substantial differences between the length of helices, the observation that S_{zz} is minimally changed in these four solution conditions, and the fact that motional quenching with magnesium has been previously observed (37,38,40). We therefore conclude that the internal motions of the HIV FS are effectively quenched by 2 mM magnesium.

Interhelical bend angles were determined from the order tensor solutions by rotating each idealized A-form helix into the principal axis system of the order tensor (S_{zz}, S_{yy}, S_{xx}). The two helices were then translated to satisfy connectivity restraints between U6 and C7 and the distance restraint between G32 and A36. Helical dynamics were assessed using two additional order tensor terms: the internal generalized degree of order (GDO_{int}) and the asymmetry parameter (η) (3,62,81). GDO_{int} describes the amplitude of interhelical motions and varies between 0 and 1, from maximum to minimum motional amplitudes, respectively. The asymmetry parameter for the two helices, η, can be compared to obtain insights into the asymmetry of motions, with large and small differences implying asymmetric and isotropic motions, respectively (19,60,67,81). Dynamics defined by no directional preference are deemed isotropic and can be modeled assuming an isotropic cone motional model (36,82–85).

In 20 mM potassium, the RNA adopts an average β of $43°(\pm 4°)$ (Fig. 3 *A*) and experiences large amplitude motions (Table 1: $GDO_{int} = 0.67(\pm 0.03)$). The differences in η values (Table 1: $\eta = 0.12(\pm 0.04)$ and $0.31(\pm 0.03)$ for the upper and lower helices, respectively) are indicative of asymmetric interhelical motions (19). Prior studies of RNA two-way junctions suggest that β for a three nucleotide bulge uniformly sampling all topologically accessible conformations should be ~55° (18,20). Thus, the measured average bend angle for the FS is consistent with highly anisotropic domain motions. Anisotropic interhelical motions have been previously observed for TAR (6). In our previous study of the HIV-1 FS RNA structure in 50 mM NaCl, we estimated an approximate bend angle of 60° (69) based on a limited number of RDCs. In this study we make use of more RDCs (41 vs. 21) and thus can more precisely define this angle as $43°(\pm 4°)$.

In comparison to the 20 mM potassium condition (Fig. 3 *A*), order tensor analysis revealed no significant

TABLE 1 Order tensor analysis of RDCs measured in the upper and lower helices in the HIV-1 FS RNA

Ionic condition	Helix	*N*	CN	rmsd (Hz)	R^2	η	GDO × 10^{-3}	GDO_{int}	β
20 mM K^+	upper	24	3.3	2.5	0.99	0.12 ± 0.04	1.67 ± 0.05	0.67 ± 0.03	43 ± 4
	lower	17	2.8	1.7	0.99	0.31 ± 0.03	1.12 ± 0.03		
150 mM K^+	upper	19	3.7	3.5	0.98	0.26 ± 0.04	2.0 ± 0.1	0.52 ± 0.04	44 ± 4
	lower	13	3.6	2.7	0.98	0.50 ± 0.1	1.04 ± 0.07		
20 mM K^+ 2 mM Mg^{2+}	upper	25	3.0	2.0	0.98	0.06 ± .02	0.94 ± 0.07	0.94 ± 0.12	27 ± 7
	lower	11	4.8	3.2	0.96	0.50 ± 0.09	1.0 ± 0.1		
150 mM K^+ 2 mM Mg^{2+}	upper	28	2.5	3.1	0.97	0.23 ± 0.03	1.20 ± 0.03	0.87 ± 0.06	15 ± 6
	lower	13	4.0	2.6	0.98	0.35 ± 0.07	1.04 ± 0.07		

Shown for each helical domain is the number of RDCs (*N*), the condition number (CN), the rmsd, the correlation coefficient (R^2) between measured and back-calculated RDCs, the order tensor asymmetry ($\eta = |S_{yy} - S_{xx}|/S_{zz}$), the generalized degree of order $\left(GDO = \sqrt{\frac{2}{3}(S_{xx}^2 + S_{yy}^2 + S_{zz}^2)}, |S_{zz}| \geq |S_{yy}| \geq |S_{xx}|\right)$, the internal generalized degree of order ($GDO_{int} = GDO_i/GDO_j$; $GDO_i < GDO_j$), and the interhelical bend angle (β). All values were generated using RAMAH (77) with errors estimated using the program AFORM-RDC (78).

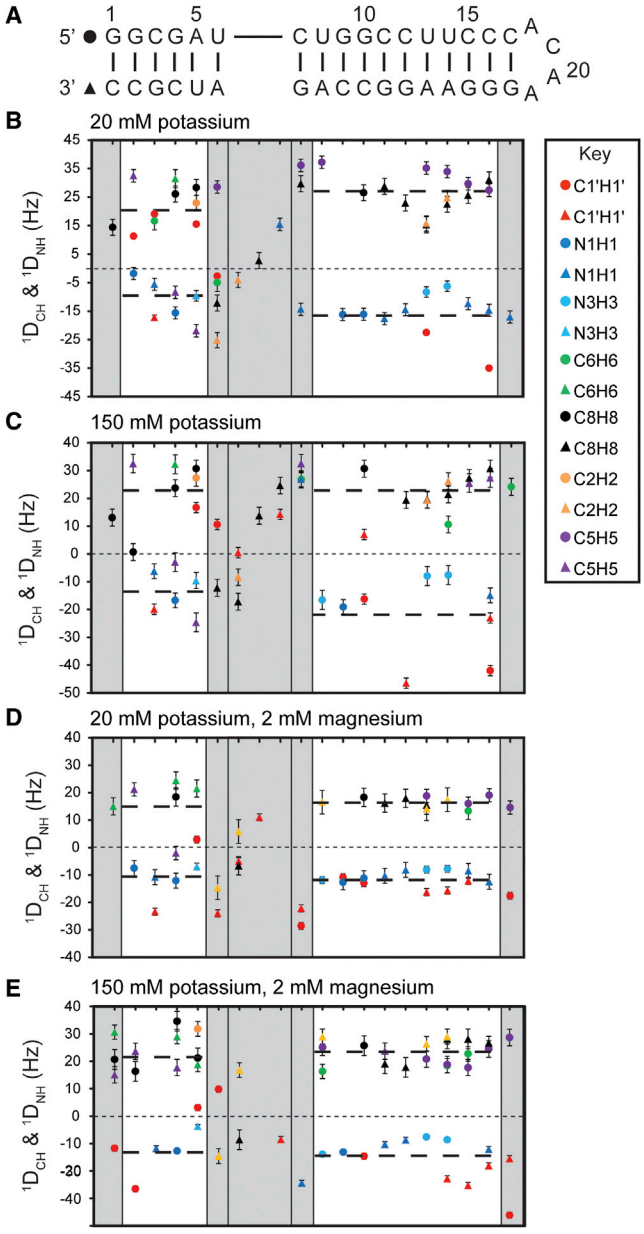

FIGURE 2 Secondary structure of the HIV-1 FS and measured RDC data. (*A*) RNA used in this study. Circles (*5′ side*) and triangles (*3′ side*) are used to distinguish RDC values measured on different sides of the helix. (*B*) RDCs values as a function of helical position. Gray sections indicate RDCs not used in order tensor analysis. The horizontal dashed lines correspond to the average positive or negative RDC value in each helix, excluding the terminal basepairs. RDCs ($^1D_{CH}$ and $^1D_{NH}$) correspond to C8-H8 (*black*), C2-H2 (*orange*), C5-H5 (*purple*), C6-H6 (*green*), N1-H1 (*dark blue*), and N3-H3 (*light blue*) spin pairs in base moieties and the C1′-H1′ (*red*) spin pair in the ribose ring in (*B*) 20 mM potassium, (*C*) 150 mM potassium, (*D*) 20 mM potassium and 2 mM magnesium, and (*E*) 150 mM potassium and 2 mM magnesium.

change in the average interhelical bend angle in 150 mM potassium (Fig. 3 *B*, Table 1). The amplitude of interhelical dynamics and motional asymmetry are similar in both conditions as well. A modest reduction in GDO_{int} and increase in η values are observed at the higher potassium concentration (Table 1), consistent with a slight increase in motional amplitude and asymmetry. A small but significant increase in FS domain dynamics and motional asymmetry was observed in 150 mM potassium relative to 20 mM potassium. Increased RNA flexibility as a function of increasing ionic strength has been previously observed for a 2-helix model RNA system using small angle x-ray scattering (86).

RDCs were measured in two different magnesium conditions (20 mM potassium and 2 mM magnesium, and 150 mM potassium and 2 mM magnesium) (Fig. 3, *C* and *D*, Table 1). In 20 mM potassium and 2 mM magnesium, the FS adopts a more coaxial orientation defined by a significant decrease in β (Fig. 3 *C*), from 43°(±4°) to 27°(±7°) (Table 1). In 150 mM potassium and 2 mM magnesium β is further decreased to 15°(±6°) (Fig. 3 *D*). Interhelical domain motions were nearly arrested by addition of magnesium (Table 1- GDO_{int} = 0.94(±0.1) and 0.87(±0.06) in 20 mM or 150 mM potassium with 2 mM magnesium, respectively). RNA structural rigidity in the presence of magnesium is consistent with previous observations for the HIV-1 TAR RNA (18,37,38,40).

Prior studies have shown that normalized resonance intensities provide a good measure of fast pico-nanosecond motions particularly for base moieties (2,42). Fast timescale dynamics in the loop nucleotides are evident from the resonance intensities observed in ^{1}H-^{13}C-HSQC experiments (Fig. 4 and Fig. S1) (2). *N*ucleotides within the tetraloop (A18, C19, A20, and A21) and bulge (A35) have intensities indicative of fast timescale motions. In each of the conditions tested, the largest normalized resonance intensities are in the tetraloop (Fig. 4). Significant tetraloop nucleotide dynamics are consistent with previous observations (87,88). The high intensity of bulge nucleotides G34 and A35 at low ionic strength is in agreement with the observed disorder in the NMR structure (69). Fast timescale motions of bulge nucleotides likely indicate that these nucleobases are only weakly stacked and may provide a flexible hinge point to facilitate the observed interdomain motions. In the presence of magnesium, many of the bulge aromatic resonances are no longer visible, indicative of intermediate exchange due to micromillisecond motions of the nucleobase, the magnesium-nucleobase interaction, or both.

Changes in bulge nucleotide stacking in response to different ionic conditions were assessed by individual substitution of the purines in the bulge with the fluorescent purine analog 2-aminopurine (2AP). Because the GGA bulge nucleotides do not participate in hydrogen bonding interactions (69), incorporation of 2AP at these positions is expected to introduce minimal structural perturbation. 2AP is a sensitive reporter of local structure because it fluoresces when solvent accessible, but is quenched upon stacking with other bases (89–99). A small number of RNA helical junctions have been experimentally analyzed in this manner (89,100). In all conditions tested, the 2AP nucleotide at

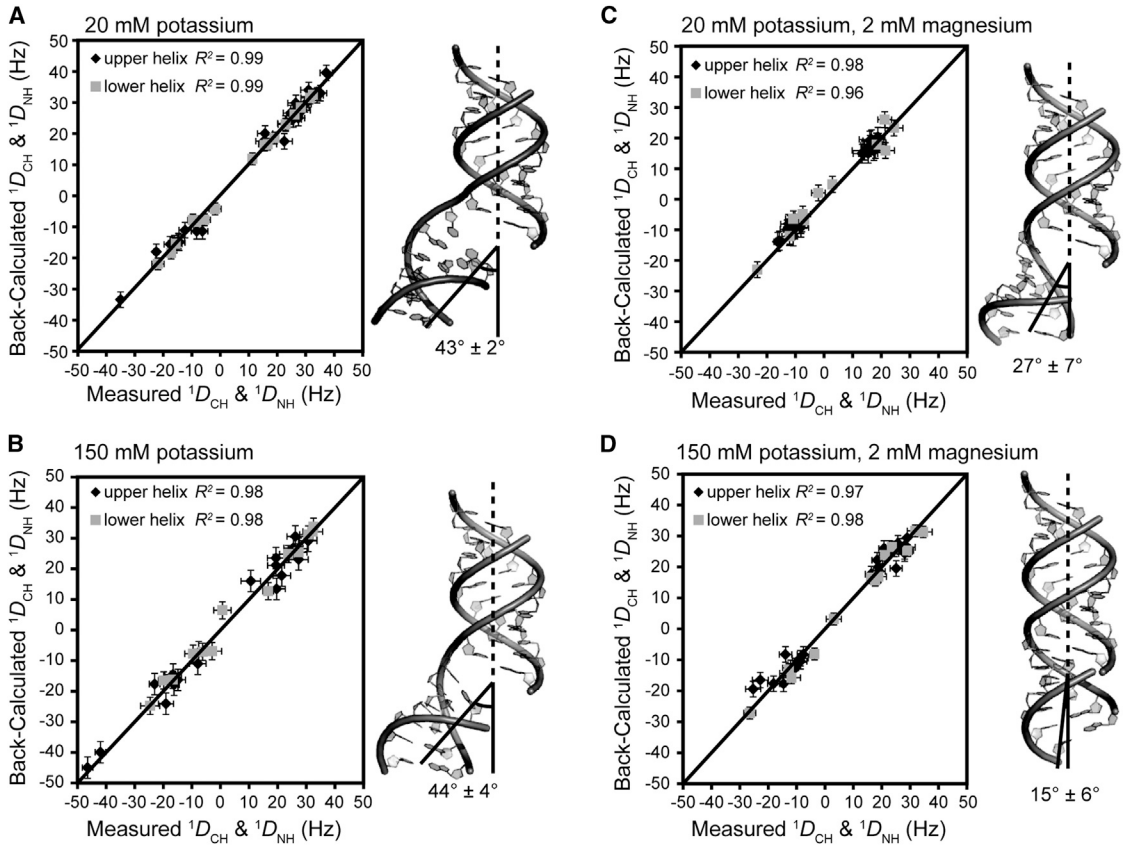

FIGURE 3 Order tensor analysis and the derived average orientations of the FS in variable potassium and magnesium concentrations. Correlation plots between measured and back-calculated RDCs when order tensors are independently fit to an idealized A-form geometry for the upper (*dark gray*) and lower (*light gray*) helices in (*A*) 20 mM potassium, (*B*) 150 mM potassium, (*C*) 20 mM potassium and 2 mM magnesium, and (*D*) 150 mM potassium and 2 mM magnesium. Error bars in the *x* axis and *y* axis are representative of the RDC measurement uncertainty (Table S1) and calculated rmsd (Table 1), respectively. In each condition, the RDC derived average orientation of the FS and interhelical bend angle is shown.

position 33 displays relatively low fluorescence (Fig. 5 *A*), consistent with a predominately stacked nucleotide conformation. This observation agrees with a favorable stacking free energy for purine nucleotides adjacent to a helical 3′ end (55) (nucleotide 33 is directly 3′ to the stable upper helix). In contrast, 2AP substitutions at nucleotides 34 and 35 display significantly higher fluorescence relative to nucleotide 33 (Fig. 5 *A*), consistent with unstacking of these bases as observed for the conformers within the ensemble of the HIV-1 FS (Fig. 5 *B*) (69).

In 20 mM potassium and 2 mM magnesium, a large increase in fluorescence is observed at position 34 (Fig. 5 *A*) indicating that magnesium promotes further unstacking of the central base in the bulge under these conditions. However, this effect is not observed in 150 mM potassium and 2 mM magnesium (Fig. 5 *A*). A possible explanation for this behavior is that the highest ionic strength condition may promote extrahelical conformations of both nucleobases 34 and 35 while inducing them to stack upon each other. A bulged conformation for both nucleotides is consistent with a conformational change related to the observed decrease in the interhelical bend angle to 15°(±6°) (Fig. 3 *D*). However, we cannot exclude the possibility that the 2-amino purine substituted RNA may respond differently to magnesium than the unmodified RNA, because 2-amino purine does not possess the electronegative O6 functional group of guanine that is often involved in magnesium ion interactions.

We examined chemical shift changes as a function of the various ionic conditions employed in this study (Fig. S2). The nucleotides around the bulge and in the tetraloop shift in a near two-state manner, whereas nucleotides in stable basepairs either do not shift (e.g., G27) or display only minor chemical shift changes (G4, A25, A26). Interestingly, the observed chemical shift changes do not track with overall ionic strength. The largest chemical shift changes are observed in 20 mM potassium and 2 mM magnesium. Upon increasing potassium concentration (150 mM potassium and 2 mM magnesium), the chemical shifts move back toward the potassium-only chemical shifts. Our 2AP fluorescence data also do not correlate with overall ionic strength, revealing that unstacking of the bulge nucleobases is greatest in 20 mM potassium and 2 mM magnesium, and that this effect is inhibited by higher concentrations of

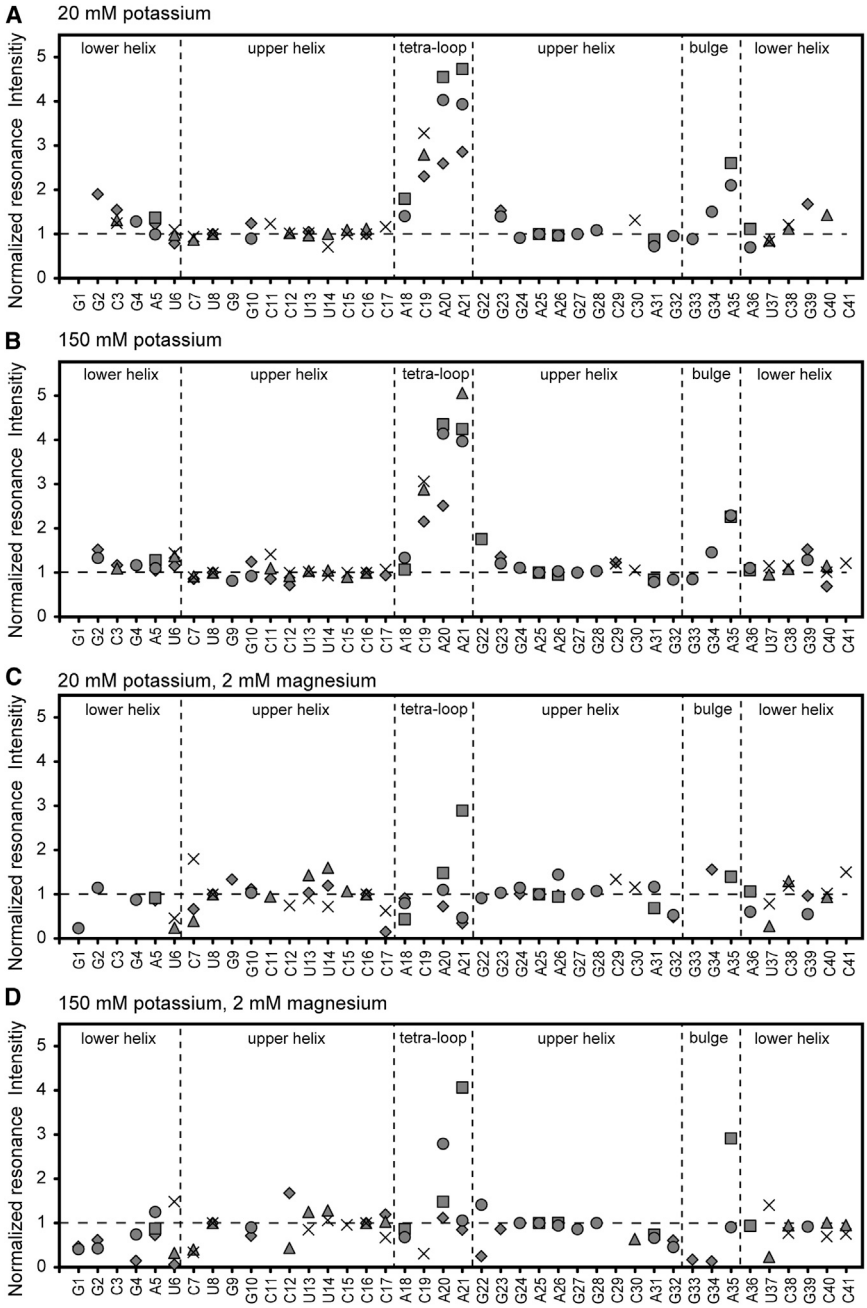

FIGURE 4 RNA dynamics measured by resonance intensities. Normalized resonance intensities (*peak heights*) measured from nonconstant-time ^{1}H-^{13}C-S^{3}A HSQC and ^{1}H-^{13}C HSQC spectra. Shown are the values for sugar C1′H1′ (*diamonds*) and base C2H2 (*squares*), C5H5 (*triangle*), C6H6 (*X*), and C8H8 (*circles*) for the FS RNA. The intensity for each type of C-H spin pair was normalized by the intensity of the corresponding A25, U8, C16, and G27 spin pairs in (*A*) 20 mM potassium, (*B*) 150 mM potassium, and (*C*) 20 mM potassium and 2 mM magnesium. (*D*) In 150 mM potassium and 2 mM magnesium cation concentrations, the intensity for each type of C-H spin pair was normalized by the intensity of the corresponding A25, U8, C16, and G24 spin pairs.

potassium (Fig. 5 *A*). It is likely that the observed chemical shifts are influenced by interactions with magnesium (40), and that these interactions are shielded by higher concentrations of potassium. In general, magnesium stabilizes base stacking as indicated by upfield ^{13}C shifts of C8 and C6 resonances (Figs. S1 and S2, *A* and *D*). As expected, the base-paired nucleotides in the helical regions all have C1′ chemical shifts diagnostic of C3′-endo sugar puckers (91.6–91.4 ppm) and aromatic resonances consistent with stacking (with the exception of the first nucleotide). The ACAA tetraloop, on the other hand, has C1′ shifts that are indicative of C2′-endo sugar puckers in potassium, consistent with the previously determined NMR structure. Upon addition of magnesium, the A20 and A21 C1' resonances shift downfield and display chemical shifts consistent with a mixture of C2' and C3′-endo sugar puckers (Figs. S1 and S2). As mentioned previously, not all resonances in the bulge could be assigned in all conditions due to intermediate exchange in the presence of magnesium. However, the C8 of G34 is shifted downfield (139.7 ppm) in 20 and 150 mM potassium (Fig. S1), which is consistent with the unstacked conformation observed in the NMR ensemble. On the other hand, the C8 of A36 shifts upfield from 140.6 ppm (20 mM potassium) to 139.7 ppm (20 mM potassium and 2 mM

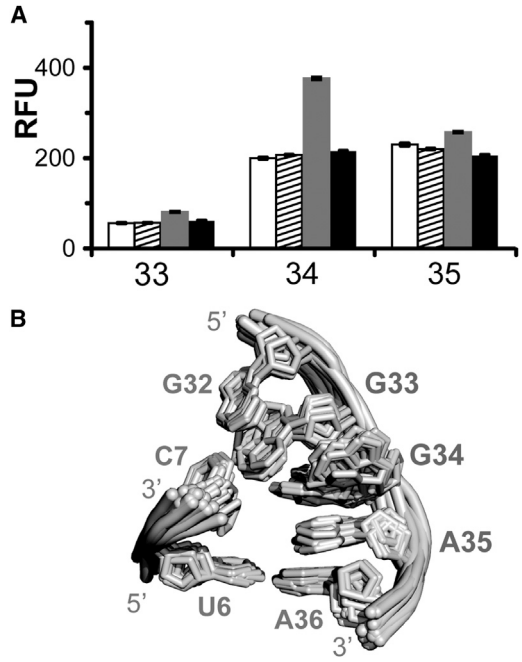

FIGURE 5 Bulge nucleotide stacking as a function of ionic conditions. (*A*) Relative fluorescence units for 2 μM RNA with 2AP incorporated at positions 33, 34, or 35 were measured in 20 mM potassium (*white*), 150 mM potassium (*hashed*), 20 mM potassium and 2 mM magnesium (*gray*), and 150 mM potassium and 2 mM magnesium (*black*) cation concentrations. Error bars representing the standard error of the mean are shown. (*B*) Ensemble of bulge conformers from the NMR structure solved in 50 mM NaCl (PDB ID 1Z2J).

magnesium), consistent with magnesium-induced stacking with the 5′ neighboring A35 base. We therefore infer that in 20 mM potassium and 2 mM Mg^{2+}, A35 is stacked on A36 and G34 is extrahelical. The A35 C8 resonance also shifts upfield from 141.7 (150 mM potassium) to 141.2 ppm in 150 mm K^{+} and 2 mM magnesium. This is consistent with A35 stacking with G34 in the highest ionic strength condition, which is in agreement with the fluorescence data. In bulge regions, magnesium appears to stabilize extrahelical nucleobase conformations by enabling the close approach of neighboring phosphate groups (16).

CONCLUSIONS

Overall, our results are remarkably similar to those that have been previously measured for TAR (2,4,6,19,20,36–46). Both RNAs have similar average interhelical bend angles (~43° (FS) and ~47° (TAR) (36)), exhibit fast timescale nucleotide dynamics in their trinucleotide bulge and loop regions (27,42,44), and display markedly anisotropic helical motions (43) that are quenched by physiological concentrations of magnesium (37,101). These results suggest that the dynamics of both RNAs are largely governed by topological constraints. Interestingly, there are also subtle differences in the dynamics of these RNAs. TAR is more flexible than the FS, with a GDO_{int} of 0.45($\pm$0.05) (43) compared to the FS GDO_{int} of 0.67($\pm$0.03). The relative decrease in flexibility for the FS may be the result of more favorable stacking interactions and possibly a greater level of steric constraints due to the purine bulge. The basepairs above and below the bulge are different for TAR and the FS and can also influence RNA dynamics (20).

Both the TAR and FS RNAs helices are coaxially aligned in physiological concentrations of magnesium (20,37,101). However, the extent of coaxial linearity is not equivalent for the two RNAs under similar ionic conditions (β = ~27° (FS, 2 mM magnesium and 20 mM potassium) versus ~5° (TAR, 2 mM magnesium and 50 mM sodium) (37)). These findings are corroborated by observations from Zacharias and Hagerman (18), which showed that helical domains connected by poly-U linkers more easily adopt coaxial conformations in the presence of divalent ions than their poly-A counterparts. The differences in extent of coaxial alignment may be attributed to the energetic penalty of purine nucleotide unstacking (59). The propensity of purine nucleotides to stack (102,103) may limit changes in interhelical orientation in response to the stabilizing effect of divalent ions (104). Therefore, the degree of flexibility in the linker may depend on its sequence, with purine-rich sequences restricting changes in interhelical orientation to a greater degree than pyrimidine-rich sequences.

The striking similarities between the HIV TAR and FS RNAs suggest that topology largely determines the conformational space of these, and perhaps many RNA junctions. However, sequence-specific effects can dramatically alter RNA dynamic behavior as previously noted (17,26). For example, there are interesting differences between our measurements and the previous work of Zacharias and Hagerman (18), in which they measured the bend angles associated with poly-A bulges in 5 mM sodium phosphate buffer, with and without 2 mM magnesium. For an AAA bulge, an interhelical bend angle of 58°($\pm$4°) is reported in both conditions (18). In contrast, we observe near-coaxial helical stacking for the FS RNA, which has a GGA bulge, in the presence of 150 mM potassium and 2 mM magnesium. The observed differences are likely due to the different bulge sequences, as magnesium ions associate much more strongly with guanines than adenines due to the ability of the electronegative O6 functional group to assist in metal ion coordination at the neighboring N7 atom (105).

SUPPORTING MATERIAL

Two figures and four tables are available at http://www.biophysj.org/biophysj/supplemental/S0006-3495(14)04749-3.

ACKNOWLEDGMENTS

The authors thank Dr. Jordan Burke, Dr. Lawrence Clos, Anthony Mustoe and Allison Didychuk for helpful discussions. Additionally, the authors thank Dr. Alessandro Senes for computational assistance.

This work was supported by National Institutes of Health (NIH) grant GM072447 to S.E.B. This study made use of the National Magnetic Resonance Facility at Madison, which is supported by NIH grants P41GM103399 (NIGMS). Equipment was purchased with funds from the University of Wisconsin-Madison, the NIH P41GM103399, S10RR02781, S10RR08438, S10RR023438, S10RR025062, S10RR029220), the NSF (DMB-8415048, OIA-9977486, BIR-9214394), and the USDA.

REFERENCES

1. Butcher, S. E., and A. M. Pyle. 2011. The molecular interactions that stabilize RNA tertiary structure: RNA motifs, patterns, and networks. *Acc. Chem. Res.* 44:1302–1311.
2. Zhang, Q., X. Sun, …, H. M. Al-Hashimi. 2006. Resolving the motional modes that code for RNA adaptation. *Science.* 311:653–656.
3. Getz, M., X. Sun, …, H. M. Al-Hashimi. 2007. NMR studies of RNA dynamics and structural plasticity using NMR residual dipolar couplings. *Biopolymers.* 86:384–402.
4. Bailor, M. H., A. M. Mustoe, …, H. M. Al-Hashimi. 2011. Topological constraints: using RNA secondary structure to model 3D conformation, folding pathways, and dynamic adaptation. *Curr. Opin. Struct. Biol.* 21:296–305.
5. Bothe, J. R., E. N. Nikolova, …, H. M. Al-Hashimi. 2011. Characterizing RNA dynamics at atomic resolution using solution-state NMR spectroscopy. *Nat. Methods.* 8:919–931.
6. Bailor, M. H., X. Sun, and H. M. Al-Hashimi. 2010. Topology links RNA secondary structure with global conformation, dynamics, and adaptation. *Science.* 327:202–206.
7. Woodson, S. A. 2010. Compact intermediates in RNA folding. *Biophys. J.* 39:61–77.
8. Liberman, J. A., and J. E. Wedekind. 2012. Riboswitch structure in the ligand-free state. *Wiley Interdiscip. Rev. RNA.* 3:369–384.
9. Liu, S., G. Bokinsky, …, X. Zhuang. 2007. Dissecting the multistep reaction pathway of an RNA enzyme by single-molecule kinetic "fingerprinting". *Proc. Natl. Acad. Sci. USA.* 104:12634–12639.
10. Chu, V. B., and D. Herschlag. 2008. Unwinding RNA's secrets: advances in the biology, physics, and modeling of complex RNAs. *Curr. Opin. Struct. Biol.* 18:305–314.
11. Dethoff, E. A., J. Chugh, …, H. M. Al-Hashimi. 2012. Functional complexity and regulation through RNA dynamics. *Nature.* 482: 322–330.
12. Hermann, T., and D. J. Patel. 1999. Stitching together RNA tertiary architectures. *J. Mol. Biol.* 294:829–849.
13. Hermann, T., and D. J. Patel. 2000. RNA bulges as architectural and recognition motifs. *Structure.* 8:R47–R54.
14. Turner, D. H. 1992. Bulges in nucleic acids. *Curr. Opin. Struct. Biol.* 2:334–337.
15. Gutell, R. R., J. J. Cannone, …, M. J. Serra. 2000. A story: unpaired adenosine bases in ribosomal RNAs. *J. Mol. Biol.* 304:335–354.
16. Salmon, L., G. Bascom, …, H. M. Al-Hashimi. 2013. A general method for constructing atomic-resolution RNA ensembles using NMR residual dipolar couplings: the basis for interhelical motions revealed. *J. Am. Chem. Soc.* 135:5457–5466.
17. Stelzer, A. C., J. D. Kratz, …, H. M. Al-Hashimi. 2010. RNA dynamics by design: biasing ensembles towards the ligand-bound state. *Angew. Chem. Int. Ed. Engl.* 49:5731–5733.
18. Zacharias, M., and P. J. Hagerman. 1995. Bulge-induced bends in RNA: quantification by transient electric birefringence. *J. Mol. Biol.* 247:486–500.
19. Zhang, Q., A. C. Stelzer, …, H. M. Al-Hashimi. 2007. Visualizing spatially correlated dynamics that directs RNA conformational transitions. *Nature.* 450:1263–1267.
20. Mustoe, A. M., M. H. Bailor, …, H. M. Al-Hashimi. 2012. New insights into the fundamental role of topological constraints as a determinant of two-way junction conformation. *Nucleic Acids Res.* 40:892–904.
21. Velculescu, V. E., L. Zhang, …, K. W. Kinzler. 1997. Characterization of the yeast transcriptome. *Cell.* 88:243–251.
22. Castle, J. C., C. Zhang, …, J. M. Johnson. 2008. Expression of 24,426 human alternative splicing events and predicted *cis* regulation in 48 tissues and cell lines. *Nat. Genet.* 40:1416–1425.
23. Pertea, M. 2012. The human transcriptome: an unfinished story. *Genes (Basel).* 3:344–360.
24. Blad, H., N. J. Reiter, …, S. E. Butcher. 2005. Dynamics and metal ion binding in the U6 RNA intramolecular stem-loop as analyzed by NMR. *J. Mol. Biol.* 353:540–555.
25. Reiter, N. J., H. Blad, …, S. E. Butcher. 2004. Dynamics in the U6 RNA intramolecular stem-loop: a base flipping conformational change. *Biochemistry.* 43:13739–13747.
26. Zhang, Q., N. K. Kim, …, J. Feigon. 2010. Structurally conserved five nucleotide bulge determines the overall topology of the core domain of human telomerase RNA. *Proc. Natl. Acad. Sci. USA.* 107:18761–18768.
27. Sun, X., Q. Zhang, and H. M. Al-Hashimi. 2007. Resolving fast and slow motions in the internal loop containing stem-loop 1 of HIV-1 that are modulated by Mg^{2+} binding: role in the kissing-duplex structural transition. *Nucleic Acids Res.* 35:1698–1713.
28. Shajani, Z., G. Drobny, and G. Varani. 2007. Binding of U1A protein changes RNA dynamics as observed by ^{13}C NMR relaxation studies. *Biochemistry.* 46:5875–5883.
29. Johnson, Jr., J. E., and C. G. Hoogstraten. 2008. Extensive backbone dynamics in the GCAA RNA tetraloop analyzed using ^{13}C NMR spin relaxation and specific isotope labeling. *J. Am. Chem. Soc.* 130:16757–16769.
30. Haller, A., M. F. Soulière, and R. Micura. 2011. The dynamic nature of RNA as key to understanding riboswitch mechanisms. *Acc. Chem. Res.* 44:1339–1348.
31. Bokinsky, G., L. G. Nivón, …, X. Zhuang. 2006. Two distinct binding modes of a protein cofactor with its target RNA. *J. Mol. Biol.* 361:771–784.
32. Grant, G. P. G., N. Boyd, …, P. Z. Qin. 2009. Motions of the substrate recognition duplex in a group I intron assessed by site-directed spin labeling. *J. Am. Chem. Soc.* 131:3136–3137.
33. Fürtig, B., J. Buck, …, H. Schwalbe. 2012. Functional dynamics of RNA ribozymes studied by NMR spectroscopy. *Methods Mol. Biol.* 848:185–199.
34. Addess, K. J., J. P. Basilion, …, A. Pardi. 1997. Structure and dynamics of the iron responsive element RNA: implications for binding of the RNA by iron regulatory binding proteins. *J. Mol. Biol.* 274:72–83.
35. Solomatin, S. V., M. Greenfeld, …, D. Herschlag. 2010. Multiple native states reveal persistent ruggedness of an RNA folding landscape. *Nature.* 463:681–684.
36. Al-Hashimi, H. M., Y. Gosser, …, D. J. Patel. 2002. Concerted motions in HIV-1 TAR RNA may allow access to bound state conformations: RNA dynamics from NMR residual dipolar couplings. *J. Mol. Biol.* 315:95–102.
37. Al-Hashimi, H. M., S. W. Pitt, …, D. J. Patel. 2003. Mg^{2+}-induced variations in the conformation and dynamics of HIV-1 TAR RNA probed using NMR residual dipolar couplings. *J. Mol. Biol.* 329:867–873.
38. Pitt, S. W., A. Majumdar, …, H. M. Al-Hashimi. 2004. Argininamide binding arrests global motions in HIV-1 TAR RNA: comparison with Mg^{2+}-induced conformational stabilization. *J. Mol. Biol.* 338:7–16.
39. Pitt, S. W., Q. Zhang, …, H. M. Al-Hashimi. 2005. Evidence that electrostatic interactions dictate the ligand-induced arrest of RNA global flexibility. *Angew. Chem. Int. Ed. Engl.* 44:3412–3415.
40. Casiano-Negroni, A., X. Sun, and H. M. Al-Hashimi. 2007. Probing $Na(^{+})$-induced changes in the HIV-1 TAR conformational dynamics

using NMR residual dipolar couplings: new insights into the role of counterions and electrostatic interactions in adaptive recognition. *Biochemistry.* 46:6525–6535.

41. Bardaro, Jr., M. F., Z. Shajani, …, G. Varani. 2009. How binding of small molecule and peptide ligands to HIV-1 TAR alters the RNA motional landscape. *Nucleic Acids Res.* 37:1529–1540.
42. Hansen, A. L., and H. M. Al-Hashimi. 2007. Dynamics of large elongated RNA by NMR carbon relaxation. *J. Am. Chem. Soc.* 129:16072–16082.
43. Dethoff, E. A., A. L. Hansen, …, H. M. Al-Hashimi. 2010. Variable helix elongation as a tool to modulate RNA alignment and motional couplings. *J. Magn. Reson.* 202:117–121.
44. Dethoff, E. A., A. L. Hansen, …, H. M. Al-Hashimi. 2008. Characterizing complex dynamics in the transactivation response element apical loop and motional correlations with the bulge by NMR, molecular dynamics, and mutagenesis. *Biophys. J.* 95:3906–3915.
45. Zhang, Q., and H. M. Al-Hashimi. 2009. Domain-elongation NMR spectroscopy yields new insights into RNA dynamics and adaptive recognition. *RNA.* 15:1941–1948.
46. Frank, A. T., A. C. Stelzer, …, I. Andricioaei. 2009. Constructing RNA dynamical ensembles by combining MD and motionally decoupled NMR RDCs: new insights into RNA dynamics and adaptive ligand recognition. *Nucleic Acids Res.* 37:3670–3679.
47. Getz, M. M., A. J. Andrews, …, H. M. Al-Hashimi. 2007. Structural plasticity and Mg^{2+} binding properties of RNase P P4 from combined analysis of NMR residual dipolar couplings and motionally decoupled spin relaxation. *RNA.* 13:251–266.
48. Dima, R. I., C. Hyeon, and D. Thirumalai. 2005. Extracting stacking interaction parameters for RNA from the data set of native structures. *J. Mol. Biol.* 347:53–69.
49. Walter, A. E., D. H. Turner, …, M. Zuker. 1994. Coaxial stacking of helixes enhances binding of oligoribonucleotides and improves predictions of RNA folding. *Proc. Natl. Acad. Sci. USA.* 91:9218–9222.
50. Mathews, D. H., J. Sabina, …, D. H. Turner. 1999. Expanded sequence dependence of thermodynamic parameters improves prediction of RNA secondary structure. *J. Mol. Biol.* 288:911–940.
51. Longfellow, C. E., R. Kierzek, and D. H. Turner. 1990. Thermodynamic and spectroscopic study of bulge loops in oligoribonucleotides. *Biochemistry.* 29:278–285.
52. Znosko, B. M., S. B. Silvestri, …, M. J. Serra. 2002. Thermodynamic parameters for an expanded nearest-neighbor model for the formation of RNA duplexes with single nucleotide bulges. *Biochemistry.* 41:10406–10417.
53. Blose, J. M., M. L. Manni, …, M. J. Serra. 2007. Non-nearest-neighbor dependence of the stability for RNA bulge loops based on the complete set of group I single-nucleotide bulge loops. *Biochemistry.* 46:15123–15135.
54. McCann, M. D., G. F. S. Lim, …, M. J. Serra. 2011. Non-nearest-neighbor dependence of the stability for RNA group II single-nucleotide bulge loops. *RNA.* 17:108–119.
55. Freier, S. M., D. Alkema, …, D. H. Turner. 1985. Contributions of dangling end stacking and terminal base-pair formation to the stabilities of XGGCCp, XCCGGp, XGGCCYp, and XCCGGYp helixes. *Biochemistry.* 24:4533–4539.
56. Sugimoto, N., R. Kierzek, and D. H. Turner. 1987. Sequence dependence for the energetics of dangling ends and terminal base pairs in ribonucleic acid. *Biochemistry.* 26:4554–4558.
57. Burkard, M. E., R. Kierzek, and D. H. Turner. 1999. Thermodynamics of unpaired terminal nucleotides on short RNA helixes correlates with stacking at helix termini in larger RNAs. *J. Mol. Biol.* 290:967–982.
58. Weeks, K. M., and D. M. Crothers. 1993. Major groove accessibility of RNA. *Science.* 261:1574–1577.
59. Barthel, A., and M. Zacharias. 2006. Conformational transitions in RNA single uridine and adenosine bulge structures: a molecular dynamics free energy simulation study. *Biophys. J.* 90:2450–2462.
60. Tolman, J. R. 2001. Dipolar couplings as a probe of molecular dynamics and structure in solution. *Curr. Opin. Struct. Biol.* 11:532–539.
61. Latham, M. P., D. J. Brown, …, A. Pardi. 2005. NMR methods for studying the structure and dynamics of RNA. *ChemBioChem.* 6:1492–1505.
62. Tolman, J. R., and K. Ruan. 2006. NMR residual dipolar couplings as probes of biomolecular dynamics. *Chem. Rev.* 106:1720–1736.
63. Low, J. T., P. Garcia-Miranda, …, K. M. Weeks. 2014. Structure and dynamics of the HIV-1 frameshift element RNA. *Biochemistry.* 53:4282–4291.
64. Bardaro, Jr., M. F., and G. Varani. 2012. Examining the relationship between RNA function and motion using nuclear magnetic resonance. *Wiley Interdiscip. Rev. RNA.* 3:122–132.
65. Tugarinov, V., Z. Liang, …, E. Meirovitch. 2001. A structural mode-coupling approach to 15N NMR relaxation in proteins. *J. Am. Chem. Soc.* 123:3055–3063.
66. Vugmeyster, L., D. P. Raleigh, …, B. E. Vugmeister. 2003. Beyond the decoupling approximation in the model free approach for the interpretation of NMR relaxation of macromolecules in solution. *J. Am. Chem. Soc.* 125:8400–8404.
67. Bailor, M. H., C. Musselman, …, H. M. Al-Hashimi. 2007. Characterizing the relative orientation and dynamics of RNA A-form helices using NMR residual dipolar couplings. *Nat. Protoc.* 2:1536–1546.
68. Mouzakis, K. D., A. L. Lang, …, S. E. Butcher. 2013. HIV-1 frameshift efficiency is primarily determined by the stability of base pairs positioned at the mRNA entrance channel of the ribosome. *Nucleic Acids Res.* 41:1901–1913.
69. Staple, D. W., and S. E. Butcher. 2005. Solution structure and thermodynamic investigation of the HIV-1 frameshift inducing element. *J. Mol. Biol.* 349:1011–1023.
70. Jacks, T., M. D. Power, …, H. E. Varmus. 1988. Characterization of ribosomal frameshifting in HIV-1 gag-pol expression. *Nature.* 331:280–283.
71. Marcheschi, R. J., K. D. Mouzakis, and S. E. Butcher. 2009. Selection and characterization of small molecules that bind the HIV-1 frameshift site RNA. *ACS Chem. Biol.* 4:844–854.
72. Gaudin, C., M.-H. Mazauric, …, D. Fourmy. 2005. Structure of the RNA signal essential for translational frameshifting in HIV-1. *J. Mol. Biol.* 349:1024–1035.
73. Dulude, D., M. Baril, and L. Brakier-Gingras. 2002. Characterization of the frameshift stimulatory signal controlling a programmed -1 ribosomal frameshift in the human immunodeficiency virus type 1. *Nucleic Acids Res.* 30:5094–5102.
74. Staple, D. W., and S. E. Butcher. 2003. Solution structure of the HIV-1 frameshift inducing stem-loop RNA. *Nucleic Acids Res.* 31:4326–4331.
75. Mollova, E. T., M. R. Hansen, and A. Pardi. 2000. Global structure of RNA determined with residual dipolar couplings. *J. Am. Chem. Soc.* 122:11561–11562.
76. Sibille, N., A. Pardi, …, M. Blackledge. 2001. Refinement of local and long-range structural order in theophylline-binding RNA using (13)C-(1)H residual dipolar couplings and restrained molecular dynamics. *J. Am. Chem. Soc.* 123:12135–12146.
77. Hansen, A. L., and H. M. Al-Hashimi. 2006. Insight into the CSA tensors of nucleobase carbons in RNA polynucleotides from solution measurements of residual CSA: towards new long-range orientational constraints. *J. Magn. Reson.* 179:299–307.
78. Musselman, C., S. W. Pitt, …, H. M. Al-Hashimi. 2006. Impact of static and dynamic A-form heterogeneity on the determination of RNA global structural dynamics using NMR residual dipolar couplings. *J. Biomol. NMR.* 36:235–249.
79. Olson, W. K., M. Bansal, …, H. M. Berman. 2001. A standard reference frame for the description of nucleic acid base-pair geometry. *J. Mol. Biol.* 313:229–237.

80. Saenger, W. 1984. Principles of nucleic acid structure. *In* Springer Advanced Texts in Chemistry. C. R. Cantor, editor. Springer-Verlag, New York, p. 557.

81. Tolman, J. R., H. M. Al-Hashimi, …, J. H. Prestegard. 2001. Structural and dynamic analysis of residual dipolar coupling data for proteins. *J. Am. Chem. Soc.* 123:1416–1424.

82. Lipari, G., and A. Szabo. 1982. Model-free approach to the interpretation of nuclear magnetic resonance relaxation in macromolecules. 2. Analysis of experimental results. *J. Am. Chem. Soc.* 104:4559–4570.

83. Meiler, J., W. Peti, and C. Griesinger. 2003. Dipolar couplings in multiple alignments suggest alpha helical motion in ubiquitin. *J. Am. Chem. Soc.* 125:8072–8073.

84. Deschamps, M., I. D. Campbell, and J. Boyd. 2005. Residual dipolar couplings and some specific models for motional averaging. *J. Magn. Reson.* 172:118–132.

85. Tolman, J. R., J. M. Flanagan, …, J. H. Prestegard. 1997. NMR evidence for slow collective motions in cyanometmyoglobin. *Nat. Struct. Biol.* 4:292–297.

86. Chu, V. B., J. Lipfert, …, D. Herschlag. 2009. Do conformational biases of simple helical junctions influence RNA folding stability and specificity? *RNA.* 15:2195–2205.

87. Staple, D. W., V. Venditti, …, S. E. Butcher. 2008. Guanidinoneomycin B recognition of an HIV-1 RNA helix. *ChemBioChem.* 9:93–102.

88. Venditti, V., N. Niccolai, and S. E. Butcher. 2008. Measuring the dynamic surface accessibility of RNA with the small paramagnetic molecule TEMPOL. *Nucleic Acids Res.* 36:e20.

89. Ballin, J. D., J. P. Prevas, …, G. M. Wilson. 2008. Local RNA conformational dynamics revealed by 2-aminopurine solvent accessibility. *Biochemistry.* 47:7043–7052.

90. Kirk, S. R., N. W. Luedtke, and Y. Tor. 2001. 2-Aminopurine as a real-time probe of enzymatic cleavage and inhibition of hammerhead ribozymes. *Bioorg. Med. Chem.* 9:2295–2301.

91. Holmén, A., B. Nordén, and B. Albinsson. 1997. Electronic transition moments of 2-aminopurine. *J. Am. Chem. Soc.* 119:3114–3121.

92. Xu, D., K. O. Evans, and T. M. Nordlund. 1994. Melting and premelting transitions of an oligomer measured by DNA base fluorescence and absorption. *Biochemistry.* 33:9592–9599.

93. Ward, D. C., E. Reich, and L. Stryer. 1969. Fluorescence studies of nucleotides and polynucleotides. I. Formycin, 2-aminopurine riboside, 2,6-diaminopurine riboside, and their derivatives. *J. Biol. Chem.* 244:1228–1237.

94. Menger, M., T. Tuschl, …, D. Porschke. 1996. $Mg(^{2+})$-dependent conformational changes in the hammerhead ribozyme. *Biochemistry.* 35:14710–14716.

95. Lacourciere, K. A., J. T. Stivers, and J. P. Marino. 2000. Mechanism of neomycin and Rev peptide binding to the Rev responsive element of HIV-1 as determined by fluorescence and NMR spectroscopy. *Biochemistry.* 39:5630–5641.

96. Hall, K. B. 2009. 2-Aminopurine as a probe of RNA conformational transitions. *In* Methods Enzymol. H. Daniel, editor. Academic Press, San Diego, CA, pp. 269–285.

97. Jean, J. M., and K. B. Hall. 2001. 2-Aminopurine fluorescence quenching and lifetimes: role of base stacking. *Proc. Natl. Acad. Sci. USA.* 98:37–41.

98. Rachofsky, E. L., R. Osman, and J. B. Ross. 2001. Probing structure and dynamics of DNA with 2-aminopurine: effects of local environment on fluorescence. *Biochemistry.* 40:946–956.

99. Rau, M., W. T. Stump, and K. B. Hall. 2012. Intrinsic flexibility of snRNA hairpin loops facilitates protein binding. *RNA.* 18:1984–1995.

100. Kim, D., S. Reddy, …, Y.-G. Kim. 2009. Base extrusion is found at helical junctions between right- and left-handed forms of DNA and RNA. *Nucleic Acids Res.* 37:4353–4359.

101. Jens, F., and K. Hans Robert. 1995. Physiological buffers for NMR spectroscopy. *J. Biomol. NMR.* 5:376–382.

102. Florian, J., J. Sponer, and A. Warshel. 1999. Thermodynamic parameters for stacking and hydrogen bonding of nucleic acid bases in aqueous solution: ab initio/Langevin dipoles study. *J. Phys. Chem. B.* 103:884–892.

103. Sponer, J., K. E. Riley, and P. Hobza. 2008. Nature and magnitude of aromatic stacking of nucleic acid bases. *Phys. Chem. Chem. Phys.* 10:2595–2610.

104. Misra, V. K., and D. E. Draper. 1998. On the role of magnesium ions in RNA stability. *Biopolymers.* 48:113–135.

105. Oliva, R., and L. Cavallo. 2009. Frequency and effect of the binding of Mg^{2+}, Mn^{2+}, and Co^{2+} ions on the guanine base in Watson-Crick and reverse Watson-Crick base pairs. *J. Phys. Chem. B.* 113:15670–15678.